Geophysical Research Letters

RESEARCH LETTER
10.1029/2020GL088853

Rapid Frequency Variations Within Intense Chorus Wave Packets

X.-J. Zhang[1], D. Mourenas[2,3], A. V. Artemyev[1], V. Angelopoulos[1], W. S. Kurth[4], C. A. Kletzing[4], and G. B. Hospodarsky[4]

[1]Department of Earth, Planetary, and Space Sciences, University of California, Los Angeles, CA, USA, [2]CEA, DAM, DIF, Arpajon, France, [3]Laboratoire Matière sous Conditions Extrêmes, Université Paris-Saclay, CEA, Bruyères-le-Châtel, France, [4]Department of Physics and Astronomy, University of Iowa, Iowa City, IA, USA

Abstract Whistler mode chorus waves are responsible for electron acceleration in Earth's radiation belts. It is unclear, however, whether the observed acceleration is still well described by quasi-linear theory, or if this acceleration is due to intense waves that require nonlinear treatment. Here, we perform a comprehensive statistical analysis of intense lower-band chorus wave packets to investigate the relationships between wave frequency variations, packet length, and wave amplitude, and their temporal variability. We find that 15% of the wave power is carried by long packets, with low frequency sweep rates (linear trend in time) that agree with the nonlinear theory of chorus wave growth. Eighty-five percent of the wave power, however, comes from short packets with large frequency variations around the linear trend. The kappa-like probability distribution of these variations is consistent with random superposition of different waves that could result in a destruction of nonlinear resonant interaction.

Key Points:
- We investigate the relationships between chorus wave frequency variations, packet length, and wave amplitude
- Fifteen percent of the wave power is carried by long packets with low frequency sweep, as predicted by nonlinear chorus wave generation theory
- Eighty-five percent of the wave power comes from packets with large frequency variations that increase as packets become shorter

Supporting Information:
- Supporting Information S1

Correspondence to:
X.-J. Zhang,
xjzhang@ucla.edu

Citation:
Zhang, X.-J., Mourenas, D., Artemyev, A. V., Angelopoulos, V., Kurth, W. S., Kletzing, C. A., & Hospodarsky, G. B. (2020). Rapid frequency variations within intense chorus wave packets. *Geophysical Research Letters*, *47*, e2020GL088853. https://doi.org/10.1029/2020GL088853

Received 15 MAY 2020
Accepted 30 JUN 2020
Accepted article online 8 JUL 2020

1. Introduction

Repeated interactions between relativistic electrons and intense whistler mode chorus waves are critical to radiation belt dynamics (Millan & Baker, 2012; Shprits et al., 2008; Thorne, 2010). In several event studies, the observed acceleration and loss of relativistic electrons, attributed to such interactions, have been successfully reproduced by quasi-linear diffusion codes (Li et al., 2014; Su et al., 2014; Thorne et al., 2013). But spacecraft observations have revealed that a significant fraction (up to 30%) of these chorus waves can reach sufficiently high amplitudes to interact with electrons in the nonlinear regime (Cattell et al., 2008; Cully et al., 2008; Tyler et al., 2019; Wilson et al., 2011; Zhang et al., 2018, 2019). Moreover, an important chorus wave property, its frequency drift, is a direct manifestation of nonlinear wave-particle interaction as a key process for wave generation (Demekhov et al., 2017; Nunn, 1974; Nunn et al., 2009; Omura et al., 2008). Such nonlinear interactions (Albert et al., 2013; Artemyev et al., 2016; Bortnik et al., 2008; Demekhov et al., 2006; Shklyar & Matsumoto, 2009) can cause the electron distribution to evolve much faster (Agapitov et al., 2015; Foster et al., 2017; Gan et al., 2020; Kurita et al., 2018). This renders the efficacy of quasi-linear diffusion theory for describing chorus interaction with electrons questionable, and its aforementioned successes in case studies paradoxical. The relative importance of quasi-linear and nonlinear interactions in radiation belt dynamics needs to be assessed using comprehensive statistics of all relevant characteristics of chorus waves.

In a statistical study of chorus waves, Teng et al. (2017) analyzed Van Allen Probes data from 2014 through 2015, visually selecting 3,577 chorus elements with long wave packets of >50 wave periods. They found that the average duration of rising-tone chorus wave elements varies with magnetic local time (MLT) and *AE* and that such elements become shorter during more active periods and in the night/dawn MLT sectors. Shue et al. (2015, 2019) analyzed the 2008–2010 waveform data from the Time History of Events and Macroscale Interactions during Substorms (THEMIS) spacecraft, examining different characteristics of chorus elements as a function of background plasma and magnetic field. In particular, Shue et al. (2019) examined characteristics of 1,329 rising-tone chorus elements, mostly long wave packets lasting >50–100 wave periods. They found that wave packet duration and normalized bandwidth (i.e., final frequency minus initial frequency) are well correlated with energetic electron temperature and density, respectively. These results are consistent with the nonlinear theory of chorus wave generation: higher temperature, temperature anisotropy, or density of energetic (3–50 keV) electrons, lead to larger wave amplitude and, therefore, a

higher frequency sweep rate, which should in turn produce shorter wave packets and a wider frequency range over a fixed period of time (Katoh & Omura, 2011; Omura & Nunn, 2011; Omura et al., 2008; Tao et al., 2017; Titova et al., 2003).

Here we expand upon these earlier statistical results by comprehensively examining the characteristics of all intense chorus wave packets, including both the relatively rare long wave packets and the much more common short wave packets (Zhang et al., 2018, 2019). Chorus wave data from the Van Allen Probes in the outer radiation belt are complemented by THEMIS data from the outer part of the inner magnetosphere beyond geostationary orbit. We analyze all waveform data and focus on the statistical distributions of frequency sweep rate, wave packet length, wave amplitude, and frequency deviations away from the apparent sweep rate. We explore the relationships between these different wave parameters in detail. The statistical distributions of wave packet characteristics that we obtain are key to an accurate assessment of wave-particle interactions in the radiation belts and throughout the inner magnetosphere.

2. Data Set and Statistical Results

Adopting the full (2012–2018) waveform data set from the Van Allen Probes outside the plasmasphere, we select all quasi-parallel (wave normal angle $<25°$) lower-band (in the $0.05–0.5\Omega_{ce}$ frequency range, where Ω_{ce} is the equatorial electron gyrofrequency) chorus wave packets, bounded by two consecutive minima (<50 pT) of the wave magnetic field amplitude (see wave packet examples in Figure 1). To exclude intervals within the plasmasphere, we use the same plasma density-based criteria as in Zhang et al. (2019) with plasma density derived from upper hybrid resonance measurements (Kurth et al., 2015) by the high-frequency receiver of the Electric and Magnetic Field Instrument Suite and Integrated Science (EMFISIS) (Kletzing et al., 2013), or from spacecraft potential measurements by the Electric Field and Waves instrument (Wygant et al., 2013). We use waveform data during the continuous burst mode of EMFISIS, lasting 6 s during each capture (at a cadence of 35,000 samples/s).

The wave half periods inside each wave packet are calculated as the intervals between two consecutive zero crossings of the wave field. Doubling these half periods, we obtain frequencies $\omega_{obs}(t)$ that are then fitted using a least squares method as $\omega_{fit}(t) = (\partial\omega/\partial t)\, t$+constant, with $\partial\omega/\partial t$ the frequency sweep rate. We focus on quasi-parallel waves due to their higher amplitudes as compared with oblique waves (Agapitov et al., 2013; Li et al., 2016). Parallel waves are often considered as the simplest example for demonstrating nonlinear effects (Gan et al., 2020; Kurita et al., 2018; Kuzichev et al., 2019; Nunn et al., 2009; Vainchtein et al., 2018). However, oblique waves also play an important role in radiation belt dynamics (Artemyev et al., 2016; Hsieh et al., 2020; Nunn & Omura, 2015; Shklyar & Matsumoto, 2009) and their structure will be worth investigating in future studies.

Statistical results are shown in Figure 2 for lower-band chorus waves: rising-tone ($\partial\omega/\partial t > 0$) waves and the less common falling-tone ($\partial\omega/\partial t < 0$) waves (Burtis & Helliwell, 1976; Burton & Holzer, 1974; Goldstein & Tsurutani, 1984; Hayakawa et al., 1990; Li et al., 2011; SantolíK et al., 2003). Figures 2a and 2b show the chorus frequency sweep rate $\partial f/\partial t$ (in kHz/s) distribution as a function of wave packet length β (in number of wave periods) and the peak amplitude $B_{w,\,peak}$ of wave packets. Although we call for simplicity $\partial f/\partial t$ the *sweep rate* for all β, the term *sweep rate* is strictly applicable only for sufficiently long packets with $\partial\omega/\partial t \ll \omega^2$ (Demekhov, 2011; Katoh & Omura, 2016; Omura et al., 2008; Tao et al., 2020). For very short wave packets, $\partial f/\partial t$ should be considered as the *global rate of variation of the average frequency*over packet duration and can be weaker than frequency fluctuations around the $(\partial f/\partial t) \approx const$ linear trend.

Note that most wave packets in Figure 2, with peak amplitudes $>70–80$ pT, are relatively well described since their wave power decreases by a factor $>2–2.5$ from their peak down to the minimum threshold level—fixed at 50 pT, a low level below which no nonlinear effects occur above the equator (Bortnik et al., 2008; Zhang et al., 2019). Sweep rates are obtained by linear regression over at least ~6–8 half-wave periods for most packets (with $\beta \geq 3–4$, see Figures 2c and 2d), corresponding to at least ~6–8 frequency points. Correlation coefficients for the large sweep rates of short packets (corresponding to a large global frequency variation over 6–20 points) are generally of the same order as for the smaller sweep rates of long packets (corresponding to a smaller global frequency variation but over more points). We further checked that sweep rates calculated over centered half packets have a similar distribution as for full packets in Figures 2a and

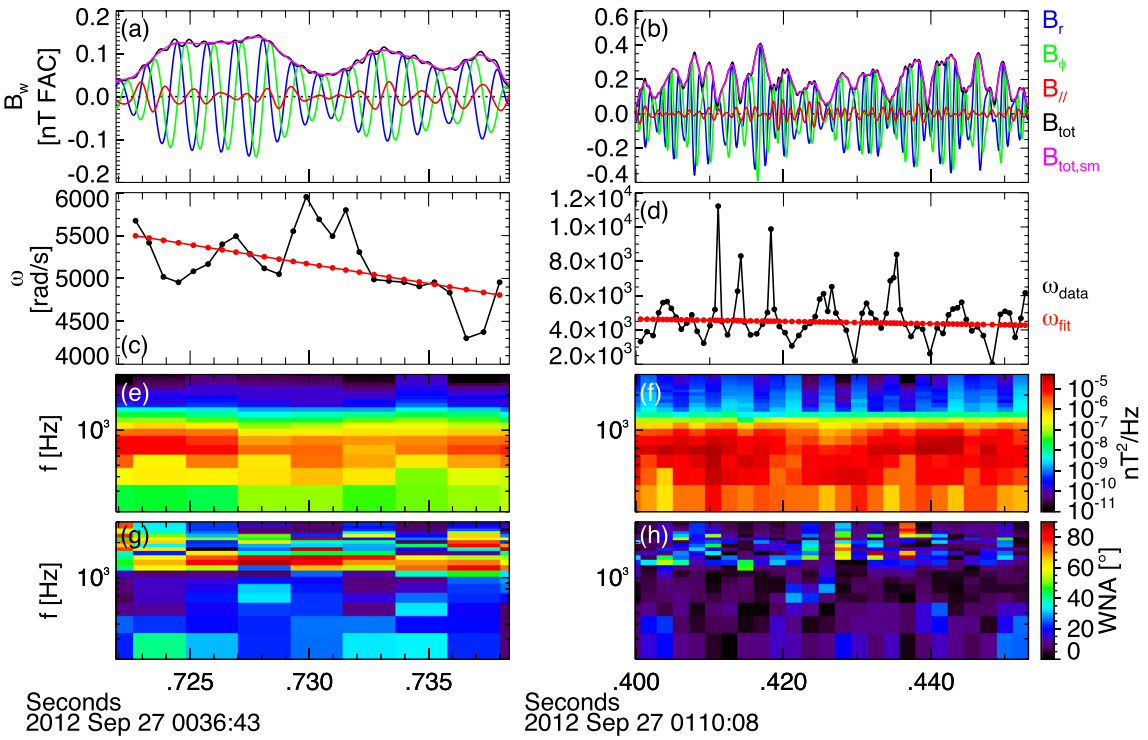

Figure 1. Two typical examples of selected short (left) and long (right) chorus wave packets. (a, b) Wave perpendicular (blue and green), parallel (red), and total magnetic field amplitude (original in black and smoothed in magenta); (c, d) observed (black) and fitted (red) wave frequency; (e, f) wave power; and (g, h) wave normal angle as a function of wave frequency.

2b, demonstrating the weak dependence of our results on the portion of packet considered (see Figure S3 in the supporting information). However, sweep rates of extremely short- ($\beta < 3$) or low-amplitude (< 70–80 pT) packets are likely less accurately determined.

For long wave packets ($\beta > 50$–100), the sweep rate $\partial f/\partial t$ generally increases with the wave amplitude from ~70 pT up to ~400–500 pT. For rising tones, $\partial f/\partial t$ reaches a plateau above 500 pT before increasing again between 1 and 3 nT, whereas it decreases above 500 pT for falling tones (> 700 pT long falling tones are rare, however). An increase of sweep rates with wave amplitude is expected from the nonlinear theory of chorus wave generation (Demekhov, 2011; Omura et al., 2008, 2013; Tao et al., 2017; Titova et al., 2003; Trakhtengerts et al., 2004) and was previously reported for rising-tone chorus packets with $\beta > 100$ (Teng et al., 2017). For rising- and falling-tone packets with $\beta > 30$–50 in our database, the measured sweep rates are $\partial f/\partial t$~0.1–10 kHz/s, with higher rates for rising tones than for falling tones, in agreement with theoretical estimates and previous studies (Cully et al., 2011; Macúšová et al., 2010; Omura et al., 2008; Tao et al., 2012; Titova et al., 2003, 2012; Trakhtengerts et al., 2004; Yamaguchi et al., 2013). For short wave packets with $\beta < 30$, however, the sweep rate $\partial f/\partial t$ increases as wave amplitude decreases from ~1 nT to ~80 pT, contrary to theoretical expectations. Moreover, for both rising- and falling-tone packets, the measured frequency sweep rates of short packets reach extremely high levels, $\partial f/\partial t$~30–200 kHz/s around 100 pT. Such sweep rates are much higher than for long wave packets in the present database, as well as in previous studies at $L > 4$ (Cully et al., 2011; Macúšová et al., 2010; Titova et al., 2003, 2012), and much higher than theoretical estimates (Omura et al., 2008; Tao et al., 2012; Trakhtengerts et al., 2004).

The contours in Figures 2a and 2b show the occurrence rate of wave packets (see caption for levels). These contours indicate that most wave packets are short ($\beta < 30$) and low amplitude (< 0.2 nT), as previously noted (Zhang et al., 2018, 2019). This implies that most wave packets (with $\beta < 30$) have extremely high sweep rates, which is inconsistent with theory. Even for long wave packets with β~50–200, in an intermediate range of amplitudes (0.25 nT $< B_{w,\,peak} < 0.6$,nT) $\partial f/\partial t$ is nearly independent of $B_{w,\,peak}$, contrary to theoretical expectations. In this range of amplitudes, sweep rates of short packets, as well as of long packets, are very similar for both rising and falling tones, which also contrasts with past observations and theory that

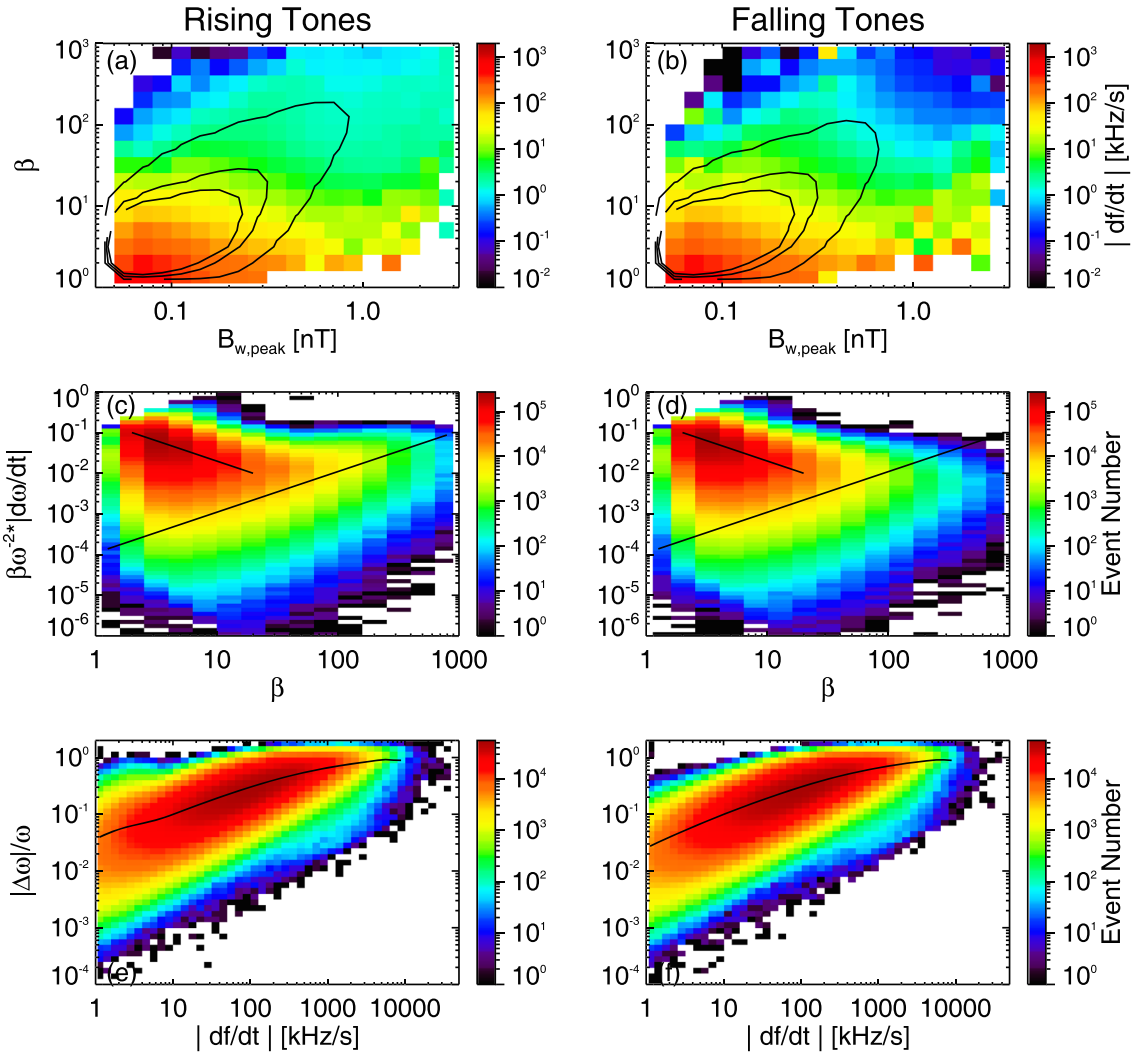

Figure 2. (a, b) Distribution of chorus frequency sweep rate, $\partial f/\partial t$ (in kHz/s), as a function of wave packet length, β (in number of wave periods $1/\langle f\rangle = 2\pi/\langle\omega\rangle$), and peak wave amplitude, $B_{w,\,peak}$, of lower-band chorus wave packets, for rising ($\partial\omega/\partial t>0$) and falling ($\partial\omega/\partial t>0$) tones. Solid black lines show contour levels of the distribution of packet occurrences (0.0005, 0.005, and 0.01 in downward direction). (c, d) Distribution of $\beta(\partial\omega/\partial t)/\langle\omega\rangle^2 = (df/\langle f\rangle)/2\pi$ as a function of packet length (β) for rising and falling tones. $\langle f\rangle$ and $\langle\omega\rangle$ denote the average wave frequency within the packet. Solid black lines show the typical variations in different parameter domains. (e, f) Distribution of the relative standard deviation of the measured frequency compared with the fitted frequency inside wave packets, $\Delta\omega/\langle\omega\rangle$, as a function of frequency sweep rate $\partial f/\partial t$, for rising and falling tones. Solid black lines show mean variations in different parameter ranges.

considered long, intense wave packets (Cully et al., 2011; Macúšová et al., 2010; Nunn & Omura, 2012; Trakhtengerts et al., 2004). Our observations suggest that the sweep rate of such short or intermediate-amplitude long wave packets may not be related to the usual nonlinear evolution of the electron distribution (hole or step formation) on which the classical theory of wave generation is based (Omura et al., 2008, 2013; Titova et al., 2003; Trakhtengerts et al., 2004).

Figures 2c and 2d show the event distribution of the normalized parameter $\beta(\partial\omega/\partial t)/\langle\omega\rangle^2$ as a function of packet length β (here $\langle\omega\rangle$ is the average wave frequency within the packet). The parameter $\beta(\partial\omega/\partial t)/\langle\omega\rangle^2 = (df/\langle f\rangle)/2\pi$ is proportional to the relative variation of the wave frequency ($df/\langle f\rangle$) over wave packet duration $\beta/\langle f\rangle$ due to the measured sweep rate $\partial f/\partial t$. In Figures 2c and 2d, $\beta(\partial\omega/\partial t)/\langle\omega\rangle^2$ most often decreases or remains constant as β increases. This indicates that wave packet length and sweep rate are anticorrelated, as previously found by Teng et al. (2017) and Shue et al. (2019) based on limited statistics of long packets (most with $\beta > 50$–100) from measurements of the Van Allen Probes and THEMIS, respectively.

For long wave packets and/or small $\partial f/\partial t$, the mean relative frequency variation ($df/\langle f\rangle$) over wave packet duration increases linearly with β from low levels, which is indicative of a frequency sweep rate independent of packet length β. The variation of $\beta(\partial\omega/\partial t)/\langle\omega\rangle^2$ as a function of β, for a fixed sweep rate $\partial f/\partial t = 5$ kHz/s typical of nonlinear chorus wave growth theory (Cully et al., 2011; Tao et al., 2012; Titova et al., 2003), is plotted in Figures 2c and 2d for $\langle\omega\rangle/\Omega_{ce} = 0.4$ at $L = 5$ (lower black line). The figures show good agreement between observations and theoretical expectations. For long rising-tone packets with $\beta > 100$, $\beta(\partial\omega/\partial t)/\langle\omega\rangle^2$ reaches an upper limit of $\simeq$0.12 that corresponds to a frequency variation $df/\langle f\rangle < 0.75$ over packet duration. This is probably due to the limited frequency range of lower-band chorus waves (Teng et al., 2017). For rising tones starting from $\omega \geq 0.2\Omega_{ce}$, this upper limit indeed corresponds to the limit $\omega < 0.45\Omega_{ce}$ imposed by strong linear and nonlinear Landau damping near $0.5\Omega_{ce}$ (Omura et al., 2009). Falling tones become rapidly more rare than rising tones as β increases above 100 for $|df/dt| > 5$ kHz/s and, as a result, do not show a similar constant upper limit.

In addition, Figures 2c and 2d reveal an intriguing characteristic of short ($\beta < 20$) wave packets. For most of them, $\beta(\partial\omega/\partial t)/\langle\omega\rangle^2$ decreases as $1/\beta$ with increasing packet length β (see upper black lines). Such behavior is not likely to be caused by the existence of a certain fixed range of wave frequency variation over packet duration (Teng et al., 2017), because the corresponding frequency range is often $df \leq 0.2\langle f\rangle$ for β~5–20, that is, lower than 6% of Ω_{ce} and much lower than the typical frequency range of lower-band chorus waves. Moreover, $\beta(\partial\omega/\partial t)/\langle\omega\rangle^2$ reaches much higher values ($\simeq 0.25$) for a number of (rising- and falling-tone) short wave packets with $\beta \sim 3$, corresponding to a very large $df/\langle f\rangle$~1.5 over the packet length.

How does one explain the characteristics of short wave packets? First, the frequency sweep rate of moderate-amplitude ($\simeq$0.08–0.2 nT) short packets shown in Figures 2a and 2b seems too high relative to the classical sweep rate in the nonlinear theory of individual chorus wave growth (Omura et al., 2008, 2013; Tao et al., 2017; Trakhtengerts et al., 2004). Second, simulations have shown variations of wave amplitude (and wave frequency) at the trapping period of electrons in the wave potential (Tao et al., 2017). But the relativistic trapping period (Omura et al., 2008; Tao et al., 2017) should remain $> 8/f$, for the most abundant packets with peak amplitudes < 150 pT at $L \leq 5.5$, assuming a reasonable resonant electron perpendicular energy at $\leq$150 keV, $\omega/\Omega_{ce} \simeq 0.3$, and plasma frequency to gyrofrequency ratio $\leq$5.5. This trapping period is significantly longer than the typical wave packet duration of $\beta/f \simeq 3/f$–$5/f$. Thus, variations driven by currents of trapped electrons seem an unlikely explanation for the observed high-frequency variations (the time scales of trapping-driven variations should probably be at least approximately half of the trapping period, still longer than the time scale of observed variations, and trapping-driven frequency variations (Tao et al., 2017) should remain small at moderate amplitudes).

These inconsistencies with theory suggests that the observed strong amplitude modulation of short wave packets could simply result from superposition of at least two coherent waves with a frequency difference, $\Delta\omega_*$—this frequency difference determining the packet duration $\beta/\langle f\rangle = 2\pi/\Delta\omega_* = 1/\Delta f_*$ (Tao et al., 2013). An average total frequency variation over packet length of the order of the frequency difference could lead to a very high sweep rate, $\langle|\partial f/\partial t|_{ws}\rangle \approx \Delta f_*/(\beta/\langle f\rangle) \approx \Delta f_*^2 \propto 1/\beta^2$. This would potentially explain the observed variation of $\beta(\partial\omega/\partial t)/\langle\omega\rangle^2$ over $2 < \beta < 20$ in Figures 2c and 2d, as well as very high sweep rates in Figures 2a and 2b. This possibility is further explored in section 3.

Figures 2e and 2f show the statistical distribution of the relative deviation of the measured frequency ($\omega_{obs}(t)$) from the fitted frequency ($\omega_{fit}(t)$) inside each wave packet, $\Delta\omega/\langle\omega\rangle$, where $\Delta\omega = \langle(\omega_{obs}(t) - \omega_{fit}(t))^2\rangle^{1/2}$, as a function of fitted frequency sweep rate $\partial f/\partial t$. The value of $\Delta\omega/\langle\omega\rangle$ often remains relatively small (< 0.05) for wave packets with moderate sweep rates, $\partial f/\partial t < 10$ kHz/s, which is consistent with nonlinear theory (Omura et al., 2008, 2013; Trakhtengerts et al., 2004). However, the standard deviation $\Delta\omega$ increases approximately as $\sim(\partial f/\partial t)^{1/2}$ (see black lines), reaching large values ($\Delta\omega/\langle\omega\rangle > 0.1$) for higher sweep rates ($\partial f/\partial t > 10$ kHz/s). This increase could be consistent with a sweep rate of $\partial\omega/\partial t \approx \Delta\omega^2 \approx \Delta\omega_*^2$ in the presence of superposed waves. It bespeaks of very fast, strong, random frequency changes inside most wave packets when $\partial f/\partial t > 10$ kHz/s, with similar $\Delta\omega$ distributions for both rising- and falling-tone waves, implying random f variations of the same magnitude for the two wave types.

For short wave packets (and those with $\partial f/\partial t > 10$–20 kHz/s or $\Delta\omega/\langle\omega\rangle > 0.05$), the above results imply superposition of coherent waves with slowly varying amplitudes and a significant average frequency difference

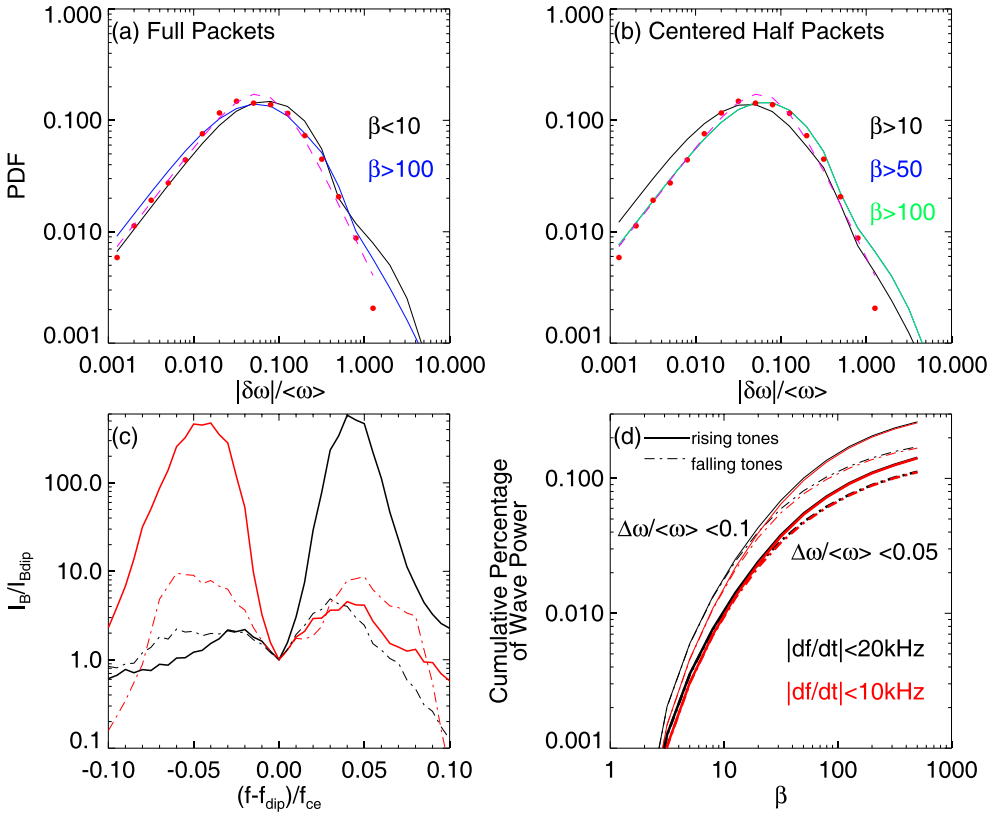

Figure 3. (a) Distribution of normalized individual deviations of measured frequency away from the fitted frequency inside chorus wave packets, $\delta\omega/\langle\omega\rangle$, for packet lengths β<10 and β>100 (in number of wave periods $1/\langle f\rangle$). The kappa distribution fit to the observed distributions is shown by a dashed magenta curve. Red dots show the statistical distribution (five points per decade) obtained from a simple model of two superposed waves, with a frequency difference $\Delta\omega_*/\Omega_{ce} \simeq 0.06$. (b) Same as (a) but over a time interval centered at each packet, with half the packet duration, for $\beta > 10$, 50, and 100. (c) Average normalized wave intensity spectrum, $I_B(f-f_{dip})/I_B(f_{dip})$, of 237 wave packets with main and secondary peaks (separated by a dip at f_{dip}), among a total number of 300 long packets ($\beta > 50$) examined where $\omega_{fit}(t) \simeq 0.3\Omega_{ce}$ varies by less than $0.015\Omega_{ce}$ (solid lines), and for 25% of such spectra with the most similar main and secondary peaks (dashed lines). (d) Cumulative probability distributions, $CDF = \sum_{\beta_* < \beta,\ \text{selected}} (\langle B_w^2\rangle \cdot \beta_*/\langle\omega\rangle) / \sum_{\text{all}} (\langle B_w^2\rangle \cdot \beta_*/\langle\omega\rangle)$, as a function of β, showing the fraction of wave power (relative to the total) with $\partial f/\partial t$<10 kHz/s (red) or 20 kHz/s (black) and $\Delta\omega/\langle\omega\rangle < 0.05$ (thick curves) or <0.1 (thin curves), separately for rising and falling tones.

Δf_*. Such superposition can indeed produce the observed packet modulation, loss of frequency coherence near the packet edges (e.g., see Figure 1), and high sweep rate $\partial f/\partial t$. For long wave packets, those with $\beta > 20$–30 and for those with $\partial f/\partial t < 10$–20 kHz/s, our observations agree with expectations from nonlinear theory of individual chorus wave growth (Omura et al., 2008, 2013; Trakhtengerts et al., 2004).

3. Statistics of Individual Frequency Deviations Inside Wave Packets

To get a deeper understanding of these results, we further examine deviations $\delta\omega = |\omega_{fit}(t) - \omega_{obs}(t)|$ of the measured frequency $\omega_{obs}(t)$ over each half wave period (i.e., black data points in Figures 1c and 1d), from the linearly fitted frequency $\omega_{fit}(t)$ within the packet (i.e., red lines in Figures 1c and 1d). Each individual deviation of frequency over a half-wave period constitutes one data point. Figure 3a shows the probability distribution function (PDF) of these individual deviations normalized to the average wave frequency over each packet, for packets with $\beta < 10$ and $\beta > 100$. This PDF is approximately a kappa distribution, $P(x) = 12.5\cdot(1+200\cdot x^2)^{-1.3}$, with $x = \delta\omega/\langle\omega\rangle$ (Livadiotis, 2015). This implies that frequency deviations are not fully random, especially for $\delta\omega/\langle\omega\rangle > 0.1$, where the long tail indicates correlations between wave frequency deviations. Strikingly, in this figure the frequency deviation PDFs for short and long wave packets are nearly the same. Figure 3b confirms these results by showing similar $\delta\omega/\langle\omega\rangle$ distributions for all packet lengths, over a time interval of half the packet duration centered in the middle of each packet.

These results lend further credence to the idea that such frequency deviations could result from superposition of waves of different frequencies, generally present inside most wave packets, whatever their length.

To test this conjecture, we adopt a simple model of short packets (Tao et al., 2013) produced by random superposition of two waves of slowly varying amplitudes, with a mean frequency $\langle\omega\rangle = 0.31\ \Omega_{ce}$ and a frequency difference $\Delta\omega_*$ (see model details in the supporting information). The PDF of $\delta\omega/\langle\omega\rangle$ from this model is plotted in Figure 3a for $\Delta\omega_*/\Omega_{ce} \simeq 0.06$, corresponding to $\beta \simeq 5$, a representative length for most short packets in Figures 2c and 2d. The model PDF is close to the observed PDF, with a similar long tail up to $\delta\omega/\langle\omega\rangle \simeq 1$. In both the model and observations (see Figure 1), the largest $\delta\omega$ occurs near the edges of the packet where the wave amplitude decreases strongly. The best agreement with the observed PDF at $\delta\omega/\langle\omega\rangle > 0.5$ is obtained for $\Delta\omega_*/\Omega_{ce} \simeq 0.06$ (smaller or larger $\Delta\omega_*$ lead to smaller PDF). In the model, the sweep rate $\langle|\partial f/\partial t|_{ws}\rangle$ due to wave superposition varies approximately as $\langle|\partial f/\partial t|_{ws}\rangle \approx \Delta f_*^2 = f^2/\beta^2$ over $0.05 < \Delta\omega_*/\Omega_{ce} < 0.08$, in agreement with statistical data in Figures 2c–2f. The model sweep rate $\langle|\partial f/\partial t|_{ws}\rangle$ increases as β decreases and can exceed the usual nonlinear sweep rate ($\partial f/\partial t \sim$5–15 kHz/s) of individual waves (Omura et al., 2008; Tao et al., 2012; Titova et al., 2012) for $\beta < 20$, as in Figures 2a and 2b. Moreover, $\langle|\partial f/\partial t|_{ws}\rangle$ reaches high values ($\sim$100 kHz/s) for $\beta \simeq 5$ and $L \simeq 5.5$, which are similar to measured sweep rates.

Based on the above results, the large frequency variations observed inside short wave packets could actually result from superposed waves with a mean frequency difference on the order of $\Delta\omega_*/\Omega_{ce} \approx 0.06$, leading to a mean packet length of $\beta \approx 5$ (similarly for rising and falling tones). Figures 3a and 3b show that 40% of the observed frequency deviations are significant ($\delta\omega/\langle\omega\rangle > 0.1$) and that 10% reach very high levels ($\delta\omega/\langle\omega\rangle > 0.3$) for both short and long packets. This suggests that long packets with $\beta >$ 30–50 should exhibit a fine structure resembling a succession of shorter packets with $\beta \sim$3–10, even though the wave envelope between them never decreases to < 50 pT. Therefore, most long packets seem to also result from superposition of several waves with a mean frequency difference on the order of $\Delta\omega_*/\Omega_{ce} \approx 0.06$.

And, indeed, Figure 3c demonstrates that wave spectra well inside long packets ($\beta > 50$) often possess a significant secondary wave power peak at $\Delta\omega_*/\Omega_{ce} \simeq 0.04$–$0.1$ from the main peak. In agreement with these results, a refined Bayesian spectral analysis of a single long wave packet (Crabtree et al., 2017) had also revealed superposed waves with a frequency difference of $\Delta\omega_*/\Omega_{ce} \approx 0.03$–$0.08$. In the case of long packets, however, a *main wave* dominates the spectrum, with a usually positive, moderate nonlinear frequency sweep rate (Crabtree et al., 2017; Cully et al., 2011; Omura et al., 2013; Shue et al., 2019; Tao et al., 2012; Titova et al., 2012). This nonlinear sweep rate is clearly revealed by linear regression inside long packets in Figures 2a and 2b, because random deviations due to additional wave superposition are mostly filtered out over such long time intervals.

In Figure 3d we estimate the fraction of time-integrated wave power, P_{NL}, with $\Delta\omega/\langle\omega\rangle < 0.05$ or 0.10 and $\partial f/\partial t <$ 10 or 20 kHz/s (the expected range of nonlinear sweep rates based on theory and past observations). This fraction of wave power should come from wave packets that are relatively less disturbed—*on average*—by strong random frequency deviations preventing efficient electron acceleration by trapping. When long packets are taken into account, P_{NL} can reach $\sim$10–15%, whereas short packets satisfying these conditions are rare. The complementary fraction of wave power, $1-P_{NL} \sim$85–90%, should correspond to a seminonlinear regime of more advective-like or diffusive-like particle scattering in energy/pitch angle, but still much faster than quasi-linear diffusion (Mourenas et al., 2018).

4. Discussion and Conclusions

Because lower-frequency chorus waves propagate at a faster group velocity, two waves generated successively near the equator by hot (3–50 keV) electrons may overlap at relatively low latitudes. The generation of two waves within the same source would require rapid variations of the unstable hot electron distribution (which provides free energy for wave growth through cyclotron resonance and wave damping through Landau resonance). Such variations could be produced by earlier interactions between previously generated wave packets and electrons at all latitudes, because electrons in cyclotron resonance travel in the direction opposite to the wave and come from higher latitudes where they have just bounced back. Electron-parallel acceleration by oblique chorus waves (Agapitov et al., 2015, 2016) or by the electric field of kinetic Alfven

waves or time domain structures (Artemyev, Rankin, & Blanco, 2015; Damiano et al., 2015; Mozer et al., 2016) could also quickly increase Landau damping or reduce temperature anisotropy, because chorus waves could overtake such Landau resonant bunches of accelerated electrons, which travel $\sim 2(1-\omega/\Omega_{ce})$ times more slowly. In agreement with this scenario, chorus wave packets become shorter on average at higher latitudes (Zhang et al., 2018), during active (high $AE > 500$ nT) periods in the night/dawn sectors (Teng et al., 2017; Zhang et al., 2018), and during periods of higher plasma beta and temperature (Shue et al., 2019; Zhang et al., 2018). This could be due to an easier generation and local superposition of waves of different frequencies during such active periods, which are characterized by strong injections of unstable hot electron populations from the plasma sheet.

Van Allen Probes observations cover the outer radiation belt up to approximately geostationary orbit, usually missing the plasma injection region at $L \sim 7$–10 in the nightside magnetosphere, where the most intense whistler mode waves are generated by highly anisotropic hot plasma sheet electrons. To generalize the results shown in Figures 2 and 3 to the plasma injection region, we supplement Van Allen Probes observations with THEMIS (Angelopoulos, 2008) measurements of chorus wave packets (see details of statistical results in the supporting information and in Zhang et al., 2018). We use magnetic field waveforms from the Search Coil Magnetometer (SCM) (Le Contel et al., 2008; Roux et al., 2008) during wave burst mode (at a cadence of 8,192 samples/s), triggered by magnetic field B_z dipolarizations (plasma injections) or by whistler wave power increases. We utilize background magnetic field data from the FGM instrument (Auster et al., 2008) to estimate the electron gyrofrequency, and plasma density is inferred from the spacecraft potential (Bonnell et al., 2008).

As shown by THEMIS measurements, distributions and model/observation comparisons from Figures 2 and 3 remain similar for $L > 6$ (see Figures S1 and S2 in the supporting information). Therefore, our results on chorus wave frequency coherence are applicable to a wide range of L shells, covering the plasma injection region and the outer radiation belt down to the plasmapause.

In summary, we have conducted comprehensive statistics of frequency variations inside lower-band chorus wave packets of all lengths, based on 6 years of Van Allen Probes data. These statistics revealed the coexistence of two populations: long wave packets with frequency sweep rate following expectations from the theory of nonlinear chorus wave generation, and short wave packets with unexpectedly large frequency variations. Most importantly, we showed that strong frequency deviations from the linear trend, larger than one-tenth of the frequency over one wave period, which may result from local superposition of waves, are ubiquitous inside wave packets of all lengths.

Note that although we required a gap of wave amplitude < 50 pT to separate wave packets, this criterion alone does not guarantee the destruction (or even significant reduction) of the efficiency of wave-particle nonlinear interaction. Indeed, phase trapped particles can travel across several nearby wave packets (Hsieh et al., 2020; Kubota & Omura, 2018). Only sufficiently large jumps of wave frequency or wave phase can ensure a destruction of such trapping (Artemyev, Mourenas, et al., 2015; Brinca, 1978; Tao et al., 2013). Although we did find significant frequency jumps inside most wave packets (often near short packets edges but also well inside long packets), a detailed quantification of their effect on nonlinear wave-particle interaction is still needed.

A succession of isolated, short wave packets with $\beta < 5$–10, consisting of superposed waves of comparable amplitudes, could lead to electron energization and scattering that resemble more quasi-linear diffusion (Andronov & Trakhtengerts, 1964; Drummond & Pines, 1962; Kennel & Engelmann, 1966; Lyons et al., 1971; Vedenov et al., 1962) than nonlinear trapping acceleration and scattering. Stochastization of relativistic particle trajectories can result from cyclotron resonance overlap for waves that are sufficiently intense, which means a wave amplitude to background magnetic field amplitude ratio $B_w/B_0 > (\Omega_{ce}/300\omega_{pe})$ for $\Delta\omega_*/\Omega_{ce} \sim 0.06$ and $\omega/\Omega_{ce} \sim 0.3$ (Chirikov, 1979; Shapiro & Sagdeev, 1997; Tao et al., 2013). Nonlinear electron acceleration can also be hindered by the very limited trapping time available inside isolated, short packets (Mourenas et al., 2018). Even with long wave packets, strong random frequency deviations could still sometimes destroy nonlinear resonance and mitigate electron acceleration by trapping, as compared with the ideal situation of electron interaction with a coherent, long packet of smoothly varying frequency (Kubota & Omura, 2018; Vainchtein et al., 2018). This could explain the success of quasi-linear diffusion codes in reproducing the observed multi-MeV electron energization during geomagnetic storms

(Glauert et al., 2014; Li et al., 2014; Shprits et al., 2015; Su et al., 2014; Thorne et al., 2013), despite the high amplitude of chorus wave packets (Zhang et al., 2019). Future test particle numerical simulations using the measured statistical distributions of frequency variations inside both short and long wave packets are required to assess actual consequences of these variations on wave-particle interactions in the radiation belts.

Data Availability Statements

THEMIS Search Coil Magnetometer data (Le Contel et al., 2008; Roux et al., 2008), fluxgate magnetometer data (Auster et al., 2008), and spacecraft potential (Bonnell et al., 2008) can be accessed from this site (https://themis.ssl.berkeley.edu/). Van Allen Probes EMFISIS data can be obtained from this site (https://emfisis.physics.uiowa.edu/data/index).

Acknowledgments
We gratefully acknowledge Van Allen Probes EMFISIS data obtained from this site (https://emfisis.physics.uiowa.edu/data/index). The work at the University of Iowa was supported by NASA through JHU/APL Contract 921647 under NASA Prime contract NAS5-01072. X. J. Z. and A. V. A. acknowledge NSF Grants 2026375 and 1914594 for support, and NASA Contract NAS5-02099 for use of data from the THEMIS mission. We thank D. E. Larson for use of SST data, K. H. Glassmeier, U. Auster, and W. Baumjohann for the FGM data provided under the lead of the Technical University of Braunschweig and with financial support through the German Ministry for Economy and Technology and the German Aerospace Center (DLR) under contract 50 OC 0302. Data analysis was done using SPEDAS V3.1, see Angelopoulos et al. (2019).

References

Agapitov, O., Artemyev, A., Krasnoselskikh, V., Khotyaintsev, Y. V., Mourenas, D., Breuillard, H., et al. (2013). Statistics of whistler mode waves in the outer radiation belt: Cluster STAFF-SA measurements. *Journal of Geophysical Research: Space Physics*, *118*, 3407–3420. https://doi.org/10.1002/jgra.50312

Agapitov, O. V., Artemyev, A. V., Mourenas, D., Mozer, F. S., & Krasnoselskikh, V. (2015). Nonlinear local parallel acceleration of electrons through Landau trapping by oblique whistler mode waves in the outer radiation belt. *Geophysical Research Letters*, *42*, 10,140–10,149. https://doi.org/10.1002/2015GL066887

Agapitov, O. V., Mourenas, D., Artemyev, A. V., & Mozer, F. S. (2016). Exclusion principle for very oblique and parallel lower band chorus waves. *Geophysical Research Letters*, *43*, 11,112–11,120. https://doi.org/10.1002/2016GL071250

Albert, J. M., Tao, X., & Bortnik, J. (2013). Aspects of nonlinear wave-particle interactions. In D. Summers, U. Mann, D. N. Baker, & M. Schulz (Eds.), *Dynamics of the Earth's radiation belts and inner magnetosphere* (pp. 255–264). Hoboken, NJ: Wiley. https://doi.org/10.1029/2012GM001324

Andronov, A. A., & Trakhtengerts, V. Y. (1964). Kinetic instability of the Earth's outer radiation belt. *Geomagnetism and Aeronomy*, *4*, 233–242.

Angelopoulos, V. (2008). The THEMIS mission. *Space Science Reviews*, *141*, 5–34. https://doi.org/10.1007/s11214-008-9336-1

Angelopoulos, V., Cruce, P., Drozdov, A., Grimes, E. W., Hatzigeorgiu, N., King, D. A., et al. (2019). The Space Physics Environment Data Analysis System (SPEDAS). *Space Science Reviews*, *215*, 9. https://doi.org/10.1007/s11214-018-0576-4

Artemyev, A., Agapitov, O., Mourenas, D., Krasnoselskikh, V., Shastun, V., & Mozer, F. (2016). Oblique whistler-mode waves in the Earth's inner magnetosphere: Energy distribution, origins, and role in radiation belt dynamics. *Space Science Reviews*, *200*, 261–355. https://doi.org/10.1007/s11214-016-0252-5

Artemyev, A. V., Mourenas, D., Agapitov, O. V., Vainchtein, D. L., Mozer, F. S., & Krasnoselskikh, V. V. (2015). Stability of relativistic electron trapping by strong whistler or electromagnetic ion cyclotron waves. *Physics of Plasmas*, *22*, 82901. https://doi.org/10.1063/1.4927774

Artemyev, A. V., Rankin, R., & Blanco, M. (2015). Electron trapping and acceleration by kinetic Alfven waves in the inner magnetosphere. *Journal of Geophysical Research: Space Physics*, *120*, 10,305–10,316. https://doi.org/10.1002/2015JA021781

Auster, H. U., Glassmeier, K. H., Magnes, W., Aydogar, O., Baumjohann, W., Constantinescu, D., et al. (2008). The THEMIS fluxgate magnetometer. *Space Science Reviews*, *141*, 235–264. https://doi.org/10.1007/s11214-008-9365-9

Bonnell, J. W., Mozer, F. S., Delory, G. T., Hull, A. J., Ergun, R. E., Cully, C. M., et al. (2008). The electric field instrument (EFI) for THEMIS. *Space Science Reviews*, *141*, 303–341. https://doi.org/10.1007/s11214-008-9469-2

Bortnik, J., Thorne, R. M., & Inan, U. S. (2008). Nonlinear interaction of energetic electrons with large amplitude chorus. *Geophysical Research Letters*, *35*, 21102. https://doi.org/10.1029/2008GL035500

Brinca, A. L. (1978). Turbulence effects in the cyclotron resonance of monochromatic whistlers. *Geophysical Research Letters*, *5*, 839–842. https://doi.org/10.1029/GL005i010p00839

Burtis, W. J., & Helliwell, R. A. (1976). Magnetospheric chorus—Occurrence patterns and normalized frequency. *Planetary Space Science*, *24*, 1007–1024. https://doi.org/10.1016/0032-0633(76)90119-7

Burton, R. K., & Holzer, R. E. (1974). The origin and propagation of chorus in the outer magnetosphere. *Journal of Geophysical Research*, *79*, 1014–1023. https://doi.org/10.1029/JA079i007p01014

Cattell, C., Wygant, J. R., Goetz, K., Kersten, K., Kellogg, P. J., von Rosenvinge, T., et al. (2008). Discovery of very large amplitude whistler-mode waves in Earth's radiation belts. *Geophysical Research Letters*, *35*, 1105. https://doi.org/10.1029/2007GL032009

Chirikov, B. V. (1979). A universal instability of many-dimensional oscillator systems. *Physics Reports*, *52*, 263–379. https://doi.org/10.1016/0370-1573(79)90023-1

Crabtree, C., Tejero, E., Ganguli, G., Hospodarsky, G., & Kletzing, C. (2017). Bayesian spectral analysis of chorus subelements from the Van Allen Probes. *Journal of Geophysical Research: Space Physics*, *122*, 6088–6106. https://doi.org/10.1002/2016JA023547

Cully, C. M., Angelopoulos, V., Auster, U., Bonnell, J., & Le Contel, O. (2011). Observational evidence of the generation mechanism for rising-tone chorus. *Geophysical Research Letters*, *38*, 1106. https://doi.org/10.1029/2010GL045793

Cully, C. M., Bonnell, J. W., & Ergun, R. E. (2008). THEMIS observations of long-lived regions of large-amplitude whistler waves in the inner magnetosphere. *Geophysical Research Letters*, *35*, L17S16. https://doi.org/10.1029/2008GL033643

Damiano, P. A., Johnson, J. R., & Chaston, C. C. (2015). Ion temperature effects on magnetotail Alfvén wave propagation and electron energization. *Journal of Geophysical Research: Space Physics*, *120*, 5623–5632. https://doi.org/10.1002/2015JA021074

Demekhov, A. G. (2011). Generation of VLF emissions with the increasing and decreasing frequency in the magnetosperic cyclotron maser in the backward wave oscillator regime. *Radiophysics and Quantum Electronics*, *53*, 609–622. https://doi.org/10.1007/s11141-011-9256-x

Demekhov, A. G., Taubenschuss, U., & Santolík, O. (2017). Simulation of VLF chorus emissions in the magnetosphere and comparison with THEMIS spacecraft data. *Journal of Geophysical Research: Space Physics*, *122*, 166–184. https://doi.org/10.1002/2016JA023057

Demekhov, A. G., Trakhtengerts, V. Y., Rycroft, M. J., & Nunn, D. (2006). Electron acceleration in the magnetosphere by whistler-mode waves of varying frequency. *Geomagnetism and Aeronomy*, *46*, 711–716. https://doi.org/10.1134/S0016793206060053

Drummond, W. E., & Pines, D. (1962). Nonlinear stability of plasma oscillations. *Nuclear Fusion Supplement*, *3*, 1049–1058.

Foster, J. C., Erickson, P. J., Omura, Y., Baker, D. N., Kletzing, C. A., & Claudepierre, S. G. (2017). Van Allen Probes observations of prompt MeV radiation belt electron acceleration in nonlinear interactions with VLF chorus. *Journal of Geophysical Research: Space Physics*, *122*, 324–339. https://doi.org/10.1002/2016JA023429

Gan, L., Li, W., Ma, Q., Albert, J. M., Artemyev, A. V., & Bortnik, J. (2020). Nonlinear interactions between radiation belt electrons and chorus waves: Dependence on wave amplitude modulation. *Geophysical Research Letters*, *47*, e2019GL085987. https://doi.org/10.1029/2019GL085987

Glauert, S. A., Horne, R. B., & Meredith, N. P. (2014). Three-dimensional electron radiation belt simulations using the BAS radiation belt model with new diffusion models for chorus, plasmaspheric hiss, and lightning-generated whistlers. *Journal of Geophysical Research: Space Physics*, *119*, 268–289. https://doi.org/10.1002/2013JA019281

Goldstein, B. E., & Tsurutani, B. T. (1984). Wave normal directions of chorus near the equatorial source region. *Journal of Geophysical Research*, *89*, 2789–2810. https://doi.org/10.1029/JA089iA05p02789

Hayakawa, M., Hattori, K., Shimakura, S., Parrot, M., & Lefeuvre, F. (1990). Direction finding of chorus emissions in the outer magnetosphereand their generation and propagation. *Planetary Space Science*, *38*, 135–137. https://doi.org/10.1016/0032-0633(90)90012-F

Hsieh, Y. K., Kubota, Y., & Omura, Y. (2020). Nonlinear evolution of radiation belt electron fluxes interacting with oblique whistler mode chorus emissions. *Journal of Geophysical Research: Space Physics*, *125*, e2019JA027465. https://doi.org/10.1029/2019JA027465

Katoh, Y., & Omura, Y. (2011). Amplitude dependence of frequency sweep rates of whistler mode chorus emissions. *Journal of Geophysical Research*, *116*, 7201. https://doi.org/10.1029/2011JA016496

Katoh, Y., & Omura, Y. (2016). Electron hybrid code simulation of whistler-mode chorus generation with real parameters in the Earth's inner magnetosphere. *Earth, Planets, and Space*, *68*(1), 192. https://doi.org/10.1186/s40623-016-0568-0

Kennel, C. F., & Engelmann, F. (1966). Velocity space diffusion from weak plasma turbulence in a magnetic field. *Physics of Fluids*, *9*, 2377–2388. https://doi.org/10.1063/1.1761629

Kletzing, C. A., Kurth, W. S., Acuna, M., MacDowall, R. J., Torbert, R. B., Averkamp, T., et al. (2013). The Electric and MagneticField Instrument Suite and Integrated Science (EMFISIS) on RBSP. *Space Science Reviews*, *179*, 127–181. https://doi.org/10.1007/s11214 -013-9993-6

Kubota, Y., & Omura, Y. (2018). Nonlinear dynamics of radiation belt electrons interacting with chorus emissions localized in longitude. *Journal of Geophysical Research: Space Physics*, *123*, 4835–4857. https://doi.org/10.1029/2017JA025050

Kurita, S., Miyoshi, Y., Kasahara, S., Yokota, S., Kasahara, Y., Matsuda, S., et al. (2018). Deformation of electron pitch angle distributions caused by upper band chorus observed by the Arase satellite. *Geophysical Research Letters*, *45*, 7996–8004. https://doi.org/10.1029/2018GL079104

Kurth, W. S., De Pascuale, S., Faden, J. B., Kletzing, C. A., Hospodarsky, G. B., Thaller, S., & Wygant, J. R. (2015). Electron densities inferred from plasma wave spectra obtained by the Waves instrument on Van Allen Probes. *Journal of Geophysical Research: Space Physics*, *120*, 904–914. https://doi.org/10.1002/2014JA020857

Kuzichev, V., Soto-Chavez, A. R., Park, J., Gerrard, A., & Spitkovsky, A. (2019). Magnetospheric chorus wave simulation with the TRISTAN-MP PIC code. *Physics of Plasmas*, *26*(7), 72901. https://doi.org/10.1063/1.5096537

Le Contel, O., Roux, A., Robert, P., Coillot, C., Bouabdellah, A., de La Porte, B., et al. (2008). First results of the THEMIS search coil magnetometers. *Space Science Reviews*, *141*, 509–534. https://doi.org/10.1007/s11214-008-9371-y

Li, W., Santolik, O., Bortnik, J., Thorne, R. M., Kletzing, C. A., Kurth, W. S., & Hospodarsky, G. B. (2016). New chorus wave properties near the equator from Van Allen Probes wave observations. *Geophysical Research Letters*, *43*, 4725–4735. https://doi.org/10.1002/2016GL068780

Li, W., Thorne, R. M., Bortnik, J., Shprits, Y. Y., Nishimura, Y., Angelopoulos, V., et al. (2011). Typical properties of rising and falling tone chorus waves. *Geophysical Research Letters*, *38*, 14103. https://doi.org/10.1029/2011GL047925

Li, W., Thorne, R. M., Ma, Q., Ni, B., Bortnik, J., Baker, D. N., et al. (2014). Radiation belt electron acceleration by chorus waves during the 17 March 2013 storm. *Journal of Geophysical Research: Space Physics*, *119*, 4681–4693. https://doi.org/10.1002/2014JA019945

Livadiotis, G. (2015). Introduction to special section on origins and properties of kappa distributions: Statistical background and properties of kappa distributions in space plasmas. *Journal of Geophysical Research: Space Physics*, *120*, 1607–1619. https://doi.org/10.1002/2014JA020825

Lyons, L. R., Thorne, R. M., & Kennel, C. F. (1971). Electron pitch-angle diffusion driven by oblique whistler-mode turbulence. *Journal of Plasma Physics*, *6*, 589–606. https://doi.org/10.1017/S0022377800006310

Macúšová, E., SantolíK, O., DécréAu, P., Demekhov, A. G., Nunn, D., Gurnett, D. A., et al. (2010). Observations of the relationship between frequency sweep rates of chorus wave packets and plasma density. *Journal of Geophysical Research*, *115*, A12257. https://doi.org/10.1029/2010JA015468

Millan, R. M., & Baker, D. N. (2012). Acceleration of particles to high energies in Earth's radiation belts. *Space Science Reviews*, *173*, 103–131. https://doi.org/10.1007/s11214-012-9941-x

Mourenas, D., Zhang, X. J., Artemyev, A. V., Angelopoulos, V., Thorne, R. M., Bortnik, J., et al. (2018). Electron nonlinear resonant interaction with short and intense parallel chorus wave packets. *Journal of Geophysical Research: Space Physics*, *123*, 4979–4999. https://doi.org/10.1029/2018JA025417

Mozer, F. S., Artemyev, A., Agapitov, O. V., Mourenas, D., & Vasko, I. (2016). Near-relativistic electron acceleration by Landau trapping in time domain structures. *Geophysical Research Letters*, *43*, 508–514. https://doi.org/10.1002/2015GL067316

Nunn, D. (1974). A self-consistent theory of triggered VLF emissions. *Planetary Space Science*, *22*, 349–378. https://doi.org/10.1016/0032-0633(74)90070-1

Nunn, D., & Omura, Y. (2012). A computational and theoretical analysis of falling frequency VLF emissions. *Journal of Geophysical Research*, *117*, 8228. https://doi.org/10.1029/2012JA017557

Nunn, D., & Omura, Y. (2015). A computational and theoretical investigation of nonlinear wave-particle interactions in oblique whistlers. *Journal of Geophysical Research: Space Physics*, *120*, 2890–2911. https://doi.org/10.1002/2014JA020898

Nunn, D., Santolik, O., Rycroft, M., & Trakhtengerts, V. (2009). On the numerical modelling of VLF chorus dynamical spectra. *Annales Geophysicae*, *27*, 2341–2359. https://doi.org/10.5194/angeo-27-2341-2009

Omura, Y., Hikishima, M., Katoh, Y., Summers, D., & Yagitani, S. (2009). Nonlinear mechanisms of lower-band and upper-band VLF chorus emissions in the magnetosphere. *Journal of Geophysical Research*, *114*, 7217. https://doi.org/10.1029/2009JA014206

Omura, Y., Katoh, Y., & Summers, D. (2008). Theory and simulation of the generation of whistler-mode chorus. *Journal of Geophysical Research*, *113*, 4223. https://doi.org/10.1029/2007JA012622

Omura, Y., & Nunn, D. (2011). Triggering process of whistler mode chorus emissions in the magnetosphere. *Journal of Geophysical Research*, *116*, A05205. https://doi.org/10.1029/2010JA016280

Omura, Y., Nunn, D., & Summers, D. (2013). Generation processes of whistler mode chorus emissions: Current status of nonlinear wave growth theory. In D. Summers, U. Mann, D. N. Baker, & M. Schulz (Eds.), *Dynamics of the Earth's Radiation Belts and Inner Magnetosphere* (pp. 243–254). Hoboken, NJ: Wiley. https://doi.org/10.1029/2012GM001347

Roux, A., Le Contel, O., Coillot, C., Bouabdellah, A., de La Porte, B., Alison, D., et al. (2008). The search coil magnetometer for THEMIS. *Space Science Reviews*, *141*, 265–275. https://doi.org/10.1007/s11214-008-9455-8

SantolíK, O., Gurnett, D. A., Pickett, J. S., Parrot, M., & Cornilleau-Wehrlin, N. (2003). Spatio-temporal structure of storm-time chorus. *Journal of Geophysical Research*, *108*, 1278. https://doi.org/10.1029/2002JA009791

Shapiro, V. D., & Sagdeev, R. Z. (1997). Nonlinear wave-particle interaction and conditions for the applicability of quasilinear theory. *Physics Reports*, *283*, 49–71. https://doi.org/10.1016/S0370-1573(96)00053-1

Shklyar, D. R., & Matsumoto, H. (2009). Oblique whistler-mode waves in the inhomogeneous magnetospheric plasma: Resonant interactions with energetic charged particles. *Surveys in Geophysics*, *30*, 55–104. https://doi.org/10.1007/s10712-009-9061-7

Shprits, Y. Y., Kellerman, A. C., Drozdov, A. Y., Spence, H. E., Reeves, G. D., & Baker, D. N. (2015). Combined convective and diffusive simulations: VERB-4D comparison with 17 March 2013 Van Allen Probes observations. *Geophysical Research Letters*, *42*, 9600–9608. https://doi.org/10.1002/2015GL065230

Shprits, Y. Y., Subbotin, D. A., Meredith, N. P., & Elkington, S. R. (2008). Review of modeling of losses and sources of relativistic electrons in the outer radiation belt II: Local acceleration and loss. *Journal of Atmospheric and Solar-Terrestrial Physics*, *70*, 1694–1713. https://doi.org/10.1016/j.jastp.2008.06.014

Shue, J. H., Nariyuki, Y., Katoh, Y., Saito, S., Kasahara, Y., Hsieh, Y. K., et al. (2015). Local time distributions of repetition periods for rising tone lower band chorus waves in the magnetosphere. *Geophysical Research Letters*, *42*, 8294–8301. https://doi.org/10.1002/2015GL066107

Shue, J. H., Nariyuki, Y., Katoh, Y., Saito, S., Kasahara, Y., Hsieh, Y. K., et al. (2019). A systematic study in characteristics of lower-band rising-tone chorus elements. *Journal of Geophysical Research: Space Physics*, *124*, 9003–9016. https://doi.org/10.1029/2019JA027368

Su, Z., Zhu, H., Xiao, F., Zheng, H., Wang, Y., Zong, Q. G., et al. (2014). Quantifying the relative contributions of substorm injections and chorus waves to the rapid outward extension of electron radiation belt. *Journal of Geophysical Research: Space Physics*, *119*, 10,023–10,040. https://doi.org/10.1002/2014JA020709

Tao, X., Bortnik, J., Albert, J. M., Thorne, R. M., & Li, W. (2013). The importance of amplitude modulation in nonlinear interactions between electrons and large amplitude whistler waves. *Journal of Atmospheric and Solar-Terrestrial Physics*, *99*, 67–72. https://doi.org/10.1016/j.jastp.2012.05.012

Tao, X., Li, W., Bortnik, J., Thorne, R. M., & Angelopoulos, V. (2012). Comparison between theory and observation of the frequency sweep rates of equatorial rising tone chorus. *Geophysical Research Letters*, *39*, L08106. https://doi.org/10.1029/2012GL051413

Tao, X., Zonca, F., & Chen, L. (2017). Identify the nonlinear wave-particle interaction regime in rising tone chorus generation. *Geophysical Research Letters*, *44*, 3441–3446. https://doi.org/10.1002/2017GL072624

Tao, X., Zonca, F., Chen, L., & Wu, Y. (2020). Theoretical and numerical studies of chorus waves: A review. *Science China Earth Sciences*, *63*(1), 78–92. https://doi.org/10.1007/s11430-019-9384-6

Teng, S., Tao, X., Xie, Y., Zonca, F., Chen, L., Fang, W. B., & Wang, S. (2017). Analysis of the duration of rising tone chorus elements. *Geophysical Research Letters*, *44*, 12,074–12,082. https://doi.org/10.1002/2017GL075824

Thorne, R. M. (2010). Radiation belt dynamics: The importance of wave-particle interactions. *Geophysical Research Letters*, *372*, 22107. https://doi.org/10.1029/2010GL044990

Thorne, R. M., Li, W., Ni, B., Ma, Q., Bortnik, J., Chen, L., et al. (2013). Rapid local acceleration of relativistic radiation-belt electrons by magnetospheric chorus. *Nature*, *504*, 411–414. https://doi.org/10.1038/nature12889

Titova, E. E., Demekhov, A. G., Kozelov, B. V., Santolik, O., Macusova, E., Rauch, J. L., et al. (2012). Properties of the magnetospheric backward wave oscillator inferred from CLUSTER measurements of VLF chorus elements. *Journal of Geophysical Research*, *117*, A08210. https://doi.org/10.1029/2012JA017713

Titova, E. E., Kozelov, B. V., Jiricek, F., Smilauer, J., Demekhov, A. G., & Trakhtengerts, V. Y. (2003). Verification of the backward wave oscillator model of VLF chorus generation using data from MAGION 5 satellite. *Annales Geophysicae*, *21*, 1073–1081. https://doi.org/10.5194/angeo-21-1073-2003

Trakhtengerts, V. Y., Demekhov, A. G., Titova, E. E., Kozelov, B. V., Santolik, O., Gurnett, D., & Parrot, M. (2004). Interpretation of Cluster data on chorus emissions using the backward wave oscillator model. *Physics of Plasmas*, *11*, 1345–1351. https://doi.org/10.1063/1.1667495

Tyler, E., Breneman, A., Cattell, C., Wygant, J., Thaller, S., & Malaspina, D. (2019). Statistical occurrence and distribution of high-amplitude whistler mode waves in the outer radiation belt. *Geophysical Research Letters*, *46*, 2328–2336. https://doi.org/10.1029/2019GL082292

Vainchtein, D., Zhang, X. J., Artemyev, A., Mourenas, D., Angelopoulos, V., & Thorne, R. M. (2018). Evolution of electron distribution driven by nonlinear resonances with intense field-aligned chorus waves. *Journal of Geophysical Research: Space Physics*, *123*, 8149–8169. https://doi.org/10.1029/2018JA025654

Vedenov, A. A., Velikhov, E., & Sagdeev, R. (1962). Quasilinear theory of plasma oscillations. *Nuclear Fusion Supplement*, *2*, 465–475.

Wilson, L. B. III, Cattell, C. A., Kellogg, P. J., Wygant, J. R., Goetz, K., Breneman, A., & Kersten, K. (2011). The properties of large amplitude whistler mode waves in the magnetosphere: Propagation and relationship with geomagnetic activity. *Geophysical Research Letters*, *38*, 17107. https://doi.org/10.1029/2011GL048671

Wygant, J. R., Bonnell, J. W., Goetz, K., Ergun, R. E., Mozer, F. S., Bale, S. D., et al. (2013). The electric field and waves instruments on the radiation belt storm probes mission. *Space Science Reviews*, *179*, 183–220. https://doi.org/10.1007/s11214-013-0013-7

Yamaguchi, K., Matsumuro, T., Omura, Y., & Nunn, D. (2013). Ray tracing of whistler-mode chorus elements: implications for generation mechanisms of rising and falling tone emissions. *Annales Geophysicae*, *31*, 665–673. https://doi.org/10.5194/angeo-31-665-2013

Zhang, X. J., Mourenas, D., Artemyev, A. V., Angelopoulos, V., Bortnik, J., Thorne, R. M., et al. (2019). Nonlinear electron interaction with intense chorus waves: Statistics of occurrence rates. *Geophysical Research Letters*, *46*, 7182–7190. https://doi.org/10.1029/2019GL083833

Zhang, X. J., Thorne, R., Artemyev, A., Mourenas, D., Angelopoulos, V., Bortnik, J., et al. (2018). Properties of intense field-aligned lower-band chorus waves: Implications for nonlinear wave-particle interactions. *Journal of Geophysical Research: Space Physics*, *123*, 5379–5393. https://doi.org/10.1029/2018JA025390